ACS APPLIED MATERIALS & INTERFACES

Research Article

Cite This: ACS Appl. Mater. Interfaces 2018, 10, 17345−17351

www.acsami.org

# Targetable Mesoporous Silica Nanoprobes for Mapping the Subcellular Distribution of $H_2Se$ in Cancer Cells

Bo Hu,[†] Ranran Cheng,[†] Xiaonan Gao, Xiaohong Pan, Fanpeng Kong, Xiaojun Liu, Kehua Xu,* and Bo Tang*

College of Chemistry, Chemical Engineering and Materials Science, Collaborative Innovation Center of Functionalized Probes for Chemical Imaging in Universities of Shandong, Key Laboratory of Molecular and Nano Probes, Ministry of Education, Shandong Provincial Key Laboratory of Clean Production of Fine Chemicals, Shandong Normal University, Jinan 250014, P. R. China

Supporting Information

**ABSTRACT:** Hydrogen selenide, a highly active reductant, is believed as a key molecule in the cytotoxicity of inorganic selenium compounds. However, the detail mechanism has hardly been studied because the distribution of $H_2Se$ in the subcellular organelles remains unclear. Herein, we exploited a series of novel targetable mesoporous silica nanoplatforms to map the distribution of $H_2Se$ in cytoplasm, lysosome, and mitochondria of cancer cells. The subcellular targeting moiety-conjugated mesoporous silica nanoparticles were assembled with a near-infrared fluorescent probe (NIR-$H_2Se$) for detecting endogenous $H_2Se$ in the corresponding organelles. The confocal fluorescence imaging of cancer cells induced by $Na_2SeO_3$ found out a higher concentration of $H_2Se$ accumulated only in mitochondria. Consequently, the $H_2Se$ burst in mitochondria-triggered mitochondrial collapse that led to cell apoptosis. Hence, the selenite-induced cytotoxicity in cancer cells associates with the alteration in mitochondrial function caused by high level of $H_2Se$. These findings provide a new way to explore the tumor cell apoptosis signaling pathways induced by $Na_2SeO_3$, meanwhile, we propose a research strategy for tracking the biomolecules in the subcellular organelles and the correlative cellular function and related disease diagnosis.

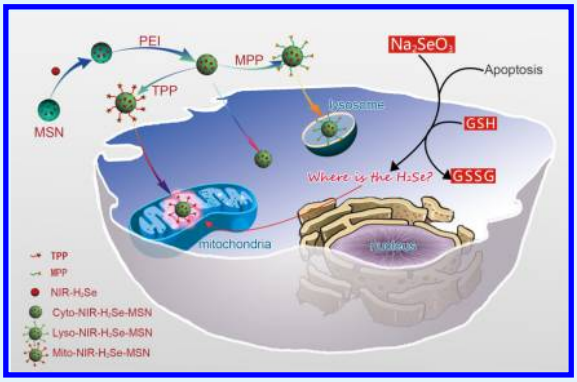


**KEYWORDS:** *$H_2Se$, mesoporous silica, subcellular organelle, $Na_2SeO_3$, hypoxic conditions*

## INTRODUCTION

The study of selenium has become research hotspot in recent years due to its excellent anticarcinogenic properties through induction of cancer cell death by different mechanisms, including DNA damage, glutathione (GSH) depletion, and protein inactivation.[1] Although these mechanisms remain elusive, recent reports demonstrated that hydrogen selenide ($H_2Se$), a common intermediate of dietary selenium metabolism,[2] is considered to influence the toxicity induced by Se compounds.[1,3] Typically, endogenous $H_2Se$ is produced by reducing selenite in the presence of in vivo thiols. As a precursor for selenol-protein synthesis or undergoes methylation to generate methylated selenium compounds, the $H_2Se$ might be involved in various biological functions in tissues and cell.[4,5] Therefore, the real-time mapping of endogenous $H_2Se$ in cancer cells is significant to understand its biological and pathological behaviors.

Moreover, the targeting and imaging subcellular organelles attract great attention in clinical applications for their crucial contribution in physiological functions and monitoring diseases.[6] Recently, to track the distribution of specific biomolecules in subcellular organelles, many novel fluorescent probes have been designed.[7] However, due to the strong reduction ability and short life time of $H_2Se$, it is difficult to detect the $H_2Se$ in vivo alone in the subcellular organelles. Wu presented a functionalized cadmium sulfide quantum dots nanosensor to detect $HSe^-$ in aqueous solution.[8] Afterward, our group designed a fluorescent probe (NIR-$H_2Se$) to detect $H_2Se$ in living cells.[9] To date, there is lack of efficient tools for real-time revealing $H_2Se$ at subcellular levels as well as mapping the distribution of $H_2Se$ in the subcellular organelles.

To fully elucidate biological functions of $H_2Se$ in cellular signaling pathways, we choose mesoporous silica nanoparticles (MSNs) as the carrier of NIR-$H_2Se$ because of their easy functionality, great biocompatibility, and high loading capacity.[10−14] Meanwhile, as the polyethylenimine (PEI), morpholines, and triphenylphosphines can target the cytoplasm, lysosome, and mitochondria respectively,[15] three targetable nanoprobes to monitor the distribution of $H_2Se$ at subcellular levels are cytoplasm (Cyto-NIR-$H_2Se$-MSN), lysosome (Lyso-NIR-$H_2Se$-MSN), and mitochondria (Mito-NIR-$H_2Se$-MSN). The PEI-, morpholine-, and triphenylphos-

Received: February 7, 2018
Accepted: April 30, 2018
Published: April 30, 2018





DOI: 10.1021/acsami.8b02206
ACS Appl. Mater. Interfaces 2018, 10, 17345−17351

phine-modified MSNs nanoplatforms could specifically target the cytoplasm, lysosomes, and mitochondria, respectively, and accurately screen the changes of $H_2Se$ in cancer cells induced by $Na_2SeO_3$ under hypoxic conditions with high selectivity and sensitivity. More significantly, in vitro study exhibits higher $H_2Se$ concentration, accumulated only in mitochondria but not in cytoplasm or lysosomes (Scheme 1). These findings offer new perspectives for future subcellular organelle studies and also greatly help the cancer therapy investigation of $Na_2SeO_3$.

**Scheme 1. Schematic Illustration of the Three Targetable Nanoprobes To Map the Subcellular Distribution of $H_2Se$ in Tumor Cells**

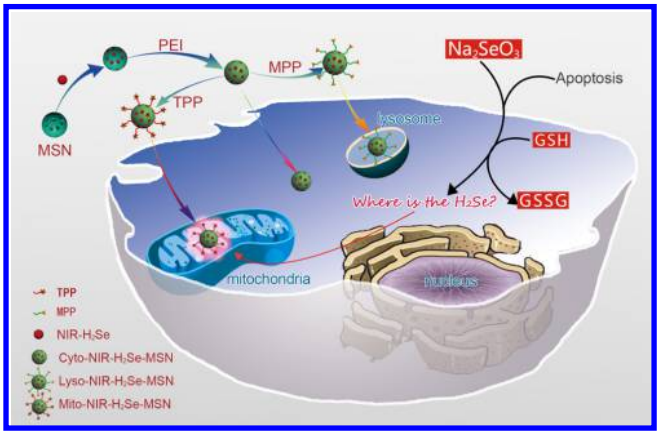


## EXPERIMENTAL SECTION

**Synthesis of the Three Nanoprobes.** MSNs (40 nm) were synthesized according to the reported method.[16] Cetyltrimethylammoniumbromide (CTAB) (0.7657 g) and tetraethylammonium (154.2 μL) were mixed in 50 mL of water, followed by intensive stirring for 30 min at 80 °C. Later tetraethoxy silane (7 mL) was added and stirred for 1 h. To remove the residual reactants, the products were washed with ethanol and methanol for several times. Finally, the products were calcined at 450 °C for 10 h to completely remove the CTAB.

NIR-$H_2Se$ (0.06 mg) was mixed with MSNs solution (1 mg/mL) and stirred at room temperature for 12 h. Excess NIR-$H_2Se$ was removed by washing the nanoparticles with water for several times. Then, PEI (0.2 mg/mL) was added to the mixture and stirred for another 24 h at room temperature in dark to activate the amino group of MSN-$NH_2$. Afterward, the solution was centrifuged for 10 min (12 000 rpm) and dispersed in the 2-(*N*-morpholino)ethanesulfonic acid (MES) (10.0 mM, pH = 6.0), resulting in the assembly of the Cyto-NIR-$H_2Se$-MSN to target cytoplasm. The as-synthesized Cyto-NIR-$H_2Se$-MSN solution (1 mL) was added to 5 μL MPP (0.1 M) and 10 μL 1-ethyl-3-(3-dimethylaminopropyl)-carbodiimide (0.1 M) solution to activate carboxylate groups, stirred at room temperature for 30 min in dark, and then *N*-hydroxysuccinimide was added (5 μL, 0.1 M). The mixture reacted at room temperature for another 24 h. The products were centrifuged and dispersed in 10.0 mM MES (pH 6.0), which finished the assembly of the Lyso-NIR-$H_2Se$-MSN to target lysosome. According to the synthetic method of Lyso-NIR-$H_2Se$-MSN above, the same method was applied, but just changed 5 μL MPP (0.1 M) with 5 μL triphenylphosphonium (0.1 M), to finally obtain the Mito-NIR-$H_2Se$-MSN to target mitochondria.

**Quantitation of NIR-$H_2Se$ Loaded on the Nanoprobes.** Nanoprobes (1 mL, 0.1 mg/mL) were heated at 70 °C for 1 h. The solution was centrifuged, and the supernatant solution was collected. Then, the precipitates were redispersed in 1 mL of phosphate-buffered saline (PBS) buffer (10.0 mM, pH 7.4) and repeated the above procedure. The fluorescence of the supernatant was excited at 688 nm and measured at 735 nm. The concentrations of NIR-$H_2Se$ were determined according to the standard linear calibration curve of NIR-$H_2Se$.

**Fluorescence Intensity (FI) Measurements.** To test the stability of the three nanoprobes under various pH values, 50 μM $H_2Se$ was added to the three nanoprobes (0.1 mg/mL) in PBS buffer (10.0 mM, pH 4–9). The fluorescence spectra were collected with $\lambda_{ex}/\lambda_{em}$ = 688/735 nm.

$H_2Se$ (0–50 μM) was added to react with the three nanoprobes (0.1 mg/mL) to detect the fluorescent response under different pH buffers (Cyto-NIR-$H_2Se$-MSN for 7.2, Lyso-NIR-$H_2Se$-MSN for 4.5, and Mito-NIR-$H_2Se$-MSN for 7.8). The fluorescence spectra were collected with $\lambda_{ex}/\lambda_{em}$ = 688/735 nm.

To evaluate the selectivity of the three nanoprobes for $H_2Se$, metal ions, oxidative-stress-associated chemicals, and amino acids were tested.[17] The concentrations applied were as follows: 50 μM for $H_2Se$, 500 μM for NO, 5 mM for other interfering substances.

The responses of the three nanoprobes to $H_2Se$ were evaluated via a kinetics experiment in different pH buffers (Cyto-NIR-$H_2Se$-MSN for 7.2, Lyso-NIR-$H_2Se$-MSN for 4.5, and Mito-NIR-$H_2Se$-MSN for 7.8). The time course for the fluorescence intensity of the nanoprobes with 25 μM $H_2Se$ was 15 min, followed by another addition of 25 μM $H_2Se$, compared with only PBS buffer (10.0 mM) at 37 °C.

**Cellular Uptake Pathways and Colocalization.** In the subcellular targeting moiety-modified nanoplatforms, a bright and acid resistance NIR fluorescent dye CF-640 was loaded, instead of NIR-$H_2Se$, to improve the veracity in the colocalization experiments.

To test the targeting time of the three nanoprobes, HepG2 cells were incubated with each nanoprobe (0.1 mg/mL) for 2, 4, 6, 8, and 10 h, then the cells were washed with PBS (pH 7.4) for three times, at last the confocal fluorescence imaging was obtained with an excitation at 633 nm.

To evaluate the availability of the three nanoprobes for subcellular location, the colocalization imaging experiments in cancer cells (HepG2, HeLa, and MCF-7 cells) were further performed. In the cytoplasm colocalization study, Cyto-CF-640-MSN (0.1 mg/mL) was incubated with the cells for 6 h, and then incubated with commercial Calcein, AM, Ultrapure Grade (CAUG, 50 nM) for 15 min. Finally, the solution was washed with PBS and examined by confocal laser scanning microscopy (CLSM). The fluorescence images were recorded in two channels. The green channel was excited at 488 nm (CAUG), the red channel was excited at 633 nm (CF-640). In the lysosomes and mitochondria colocalization studies, 0.1 mg/mL of Lyso-CF-640-MSN or Mito-CF-640-MSN, respectively, was incubated with cells for 6 h, then washed, and incubated with Lyso-Tracker DND-26 (LTD, 100 nM) or Mito-Tracker Green, respectively, (MTG, 100 nM) for 15 min. Similarly, the solution was washed with PBS for three times, and the CLSM image of stained cells was also captured using two channels.

The cellular uptake pathways were investigated: inhibit macropinocytosis by cytochalasin D (30 mM); inhibit caveolae-mediated endocytosis by genistein (1 mg/mL); inhibit clathrin-mediated uptake by chlorpromazine (10 mg/mL); and inhibit the above two endocytosis processes by dynasore (80 mM).[18−23] The cells were incubated with the inhibitors for 30 min, then incubated with 0.1 mg/mL of the three nanoprobes for 6 h at 37 °C. The fluorescence images were excited at 633 nm and collected between 650 and 750 nm. The fluorescence intensity (FI) was an average value for the cells area from the confocal fluorescence images.

**Fluorescence Imaging of $H_2Se$ at the Subcellular Level Induced by $Na_2SeO_3$.** $Na_2SeO_3$ could induce the apoptosis of cancer cell, and then it was chosen to be the $H_2Se$ precursor.[24−27] Three types of tumor cells, HepG2, HeLa, and MCF-7, were chosen in the following experiments. The cells were incubated with 0–10 μM $Na_2SeO_3$ for 12 h or 5 μM $Na_2SeO_3$ for 0–12 h, and then incubated with each nanoprobe (0.1 mg/mL) in hypoxic environments.[28] The fluorescence images were excited at 633 nm and collected between 650 and 750 nm.

**Mitochondrial Membrane Potential (MMP) Analysis.** HepG2, HeLa, and MCF-7 cells were chosen in the following experiments. Mitochondrial membrane potential ($\Delta\psi m$) was detected via staining


DOI: 10.1021/acsami.8b02206
ACS Appl. Mater. Interfaces 2018, 10, 17345−17351

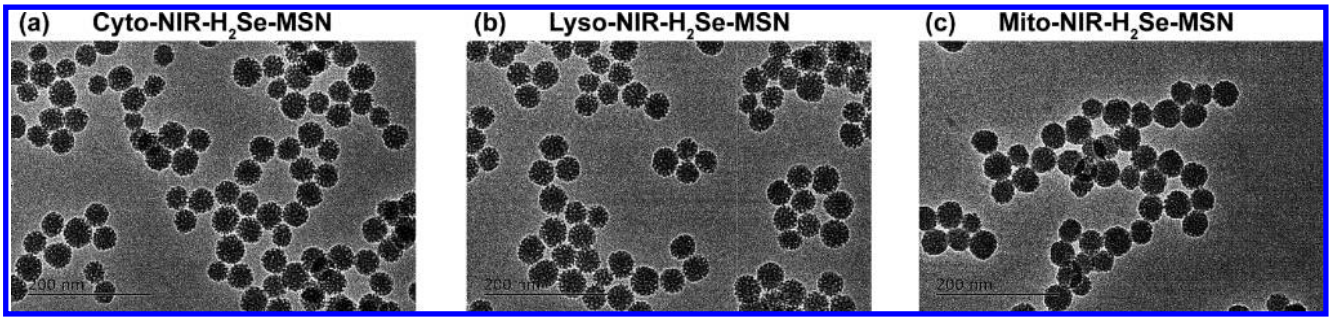


**Figure 1.** (a) Cyto-NIR-$H_2Se$-MSN, (b) Lyso-NIR-$H_2Se$-MSN, and (c) Mito-NIR-$H_2Se$-MSN were characterized by high-resolution transmission electron microscopy (HRTEM). Scale bars are 200 nm.

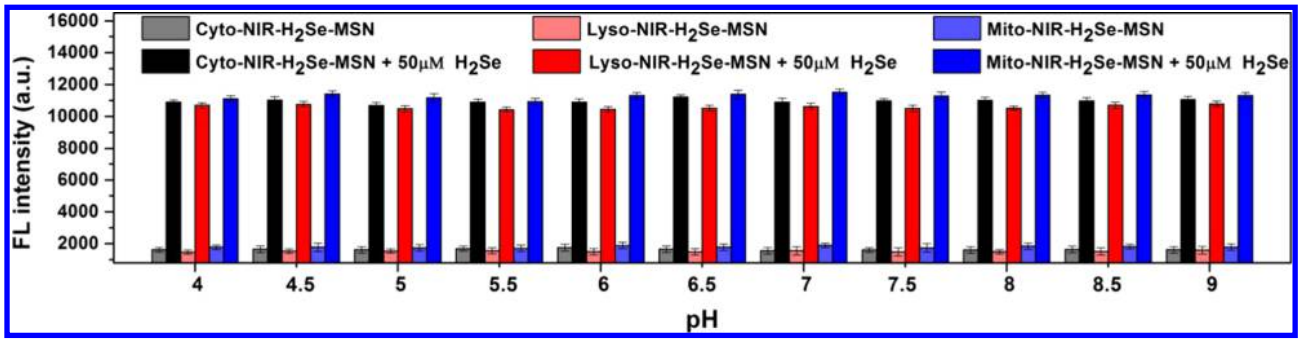


**Figure 2.** Fluorescence intensity changes of nanoprobes (0.1 mg/mL) at different pH values (pH 4−9) after addition of 50 $\mu$M $H_2Se$ in PBS buffer.

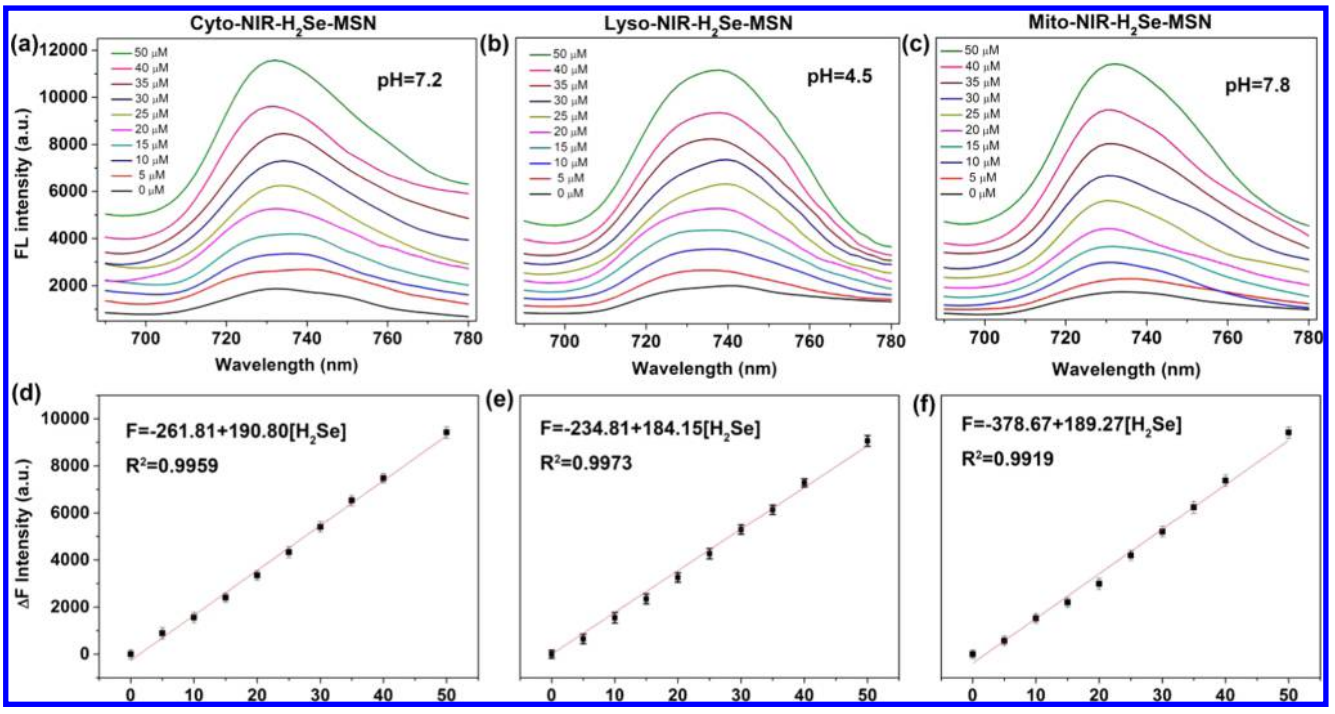


**Figure 3.** (a−c) Fluorescence changes of the three nanoprobes (0.1 mg/mL) toward various concentrations of $H_2Se$ (0−50 $\mu$M) at 37 °C in different pH buffers. (d−f) The linear correlations between the concentrations of $H_2Se$ and the fluorescence intensities of the nanoprobes at the 735 nm peak. (a, d) Cyto-NIR-$H_2Se$-MSN, (b, e) Lyso-NIR-$H_2Se$-MSN, (c, f) Mito-NIR-$H_2Se$-MSN ($F_0$ is the fluorescence intensity of the nanoprobe without $H_2Se$, $\Delta F = F - F_0$).

with rhodamine 123.[29] The tumor cells were first incubated with 0−10 $\mu$M $Na_2SeO_3$ for 12 h or 10 $\mu$M $Na_2SeO_3$ for 0−12 h under hypoxic condition, and then washed and incubated with Mito-NIR-$H_2Se$-MSN for 6 h. Afterward, the cells were stained with rhodamine 123 for 10 min, and washed with PBS. The CLSM image was captured using two channels with the same set as previous.

## RESULTS AND DISCUSSION

First, the MSNs and the $H_2Se$-responded small-molecule fluorescent probe (NIR-$H_2Se$) were synthesized according to previous literature with certain modifications (Figures S1 and S2).[9,16] Then, NIR-$H_2Se$, PEI, and targeting moiety were modified onto the MSNs in sequence to form the nanoprobes.


DOI: 10.1021/acsami.8b02206
ACS Appl. Mater. Interfaces 2018, 10, 17345−17351

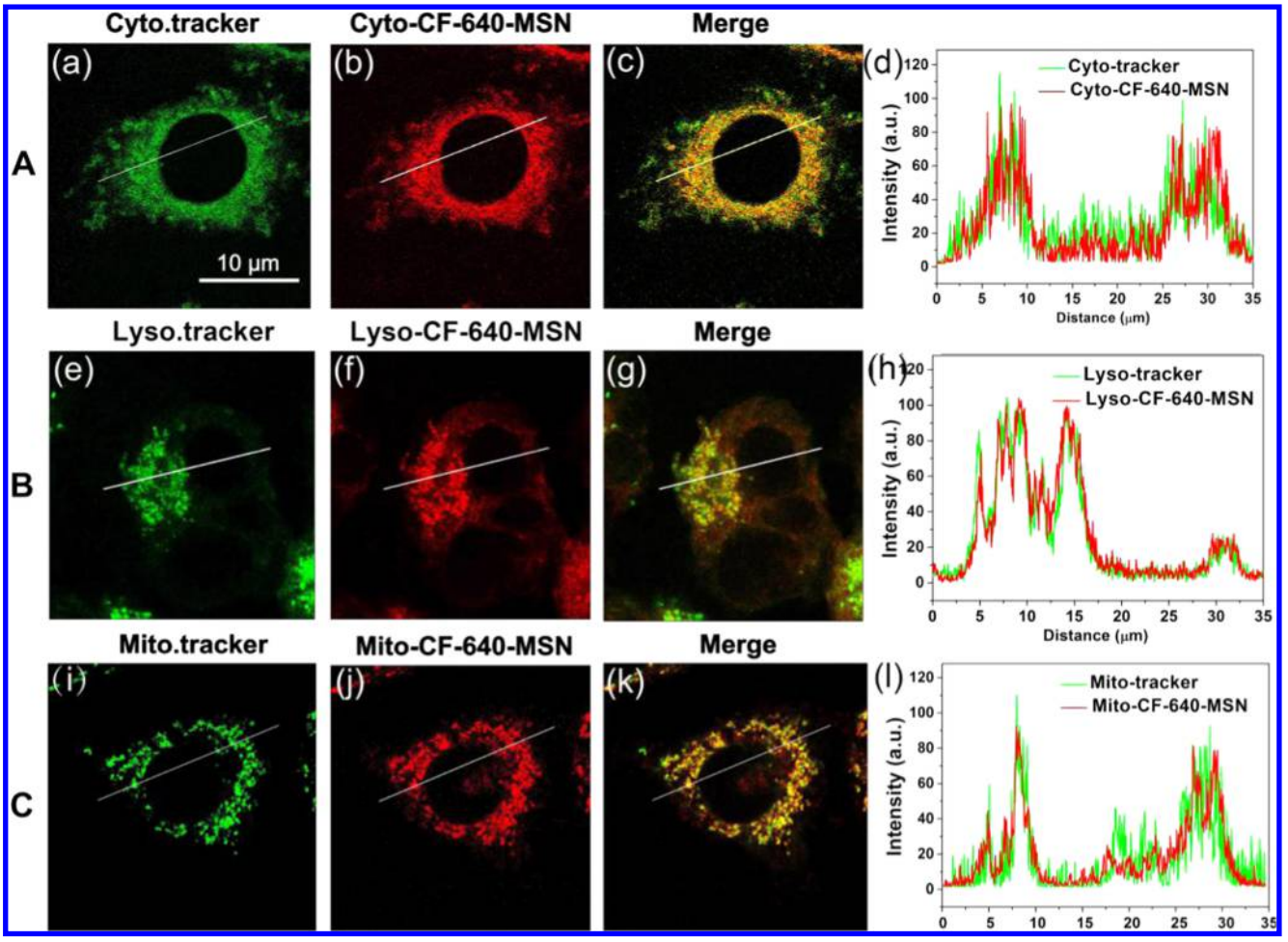


**Figure 4.** Intracellular localizations of (A) Cyto-CF-640-MSN, (B) Lyso-CF-640-MSN, (C) Mito-CF-640-MSN in HepG2 cells. The green channels of (a), (e), and (i) correspond to CA, LTG, and MTG respectively. The red channels of (b), (f), and (j) are for Cyto-CF-640-MSN, Lyso-CF-640-MSN, and Mito-CF-640-MSN respectively. (c), (g), and (k) are the corresponding merged images. (d), (h), and (l) are the fluorescence intensity profiles of regions of interest across the line.

The sizes of the three nanoprobes (Cyto-NIR-$H_2Se$-MSN, Lyso-NIR-$H_2Se$-MSN, and Mito-NIR-$H_2Se$-MSN) are approximately 40 nm and their morphologies stay spherical (Figure 1). 0.6 mg/g NIR-$H_2Se$ was loaded into the pore of the MSNs (Figure S3). Moreover, $\zeta$ potential changes in Figure S4 display a successful assembly of the nanoprobe step by step.

Fluorescence responses of the subcellular targeting nanoprobes for $H_2Se$ were tested. Considering the different pH values in each organelle, the cytoplasm for 7.2,[30−32] the lysosome for 4.5,[33−35] and the mitochondria for 7.8,[36,37] the stabilities of the three nanoprobes in different PBS buffers (pH ranges from 4 to 9) were investigated, which almost cover the physiological pH ranges (Figure 2). The increasing fluorescence intensity of the nanoprobes could be observed after addition of $H_2Se$, without significant variances at different pH values. These results demonstrate that the three nanoprobes could respond toward $H_2Se$ without pH interference in different organelles.

The fluorescence responses of the three nanoprobes for different concentrations of $H_2Se$ were studied in different pH buffers (Cyto-NIR-$H_2Se$-MSN is 7.2, Lyso-NIR-$H_2Se$-MSN is 4.5, and Mito-NIR-$H_2Se$-MSN is 7.8), which were consistent with corresponding organelles (Figure 3). Each nanoprobe exhibited remarkably fluorescence enhancement when $H_2Se$ was added and a positive linearity between the $H_2Se$ concentration and fluorescence intensity. In addition, the kinetics experiment revealed that the nanoprobes could real-time monitor $H_2Se$ because the rapid responds to $H_2Se$ can be completed in corresponding pH buffer (Figure S5).

The selectivity of the nanoprobes toward $H_2Se$ was studied by comparing with the background fluorescence. In Figure S6, the fluorescence change of the nanoprobes was not obviously in the presence of all other substances, demonstrating that every nanoprobe could selectively recognize $H_2Se$ under corresponding physiological conditions.

The cytotoxicity of the nanoprobes was also verified in HepG2 cells and HL-7702 liver cell line via MTT assay, which confirmed the low toxicity of the three nanoprobes for living cells detection (Figures S7 and S8). First, the incubating time of the nanoprobes to HepG2 cells was optimized, and the fluorescence intensity of HepG2 cells incubated with the nanoprobe reached a plateau after 6 h (Figure S9). Afterward, the uptake pathways of the nanoprobes were explored in HepG2 cells. The results suggested that endocytosis was the main uptake pathway of the nanoprobes in HepG2 cells (Figure S10).

The cellular localization experiments were performed with CLSM to confirm the intracellular location of the three nanoprobes. Because $H_2Se$ is an intermediate of selenite metabolism, for the cancer cells without treatment of $Na_2SeO_3$, the background fluorescence intensity of the nanoprobes is


DOI: 10.1021/acsami.8b02206
ACS Appl. Mater. Interfaces 2018, 10, 17345−17351

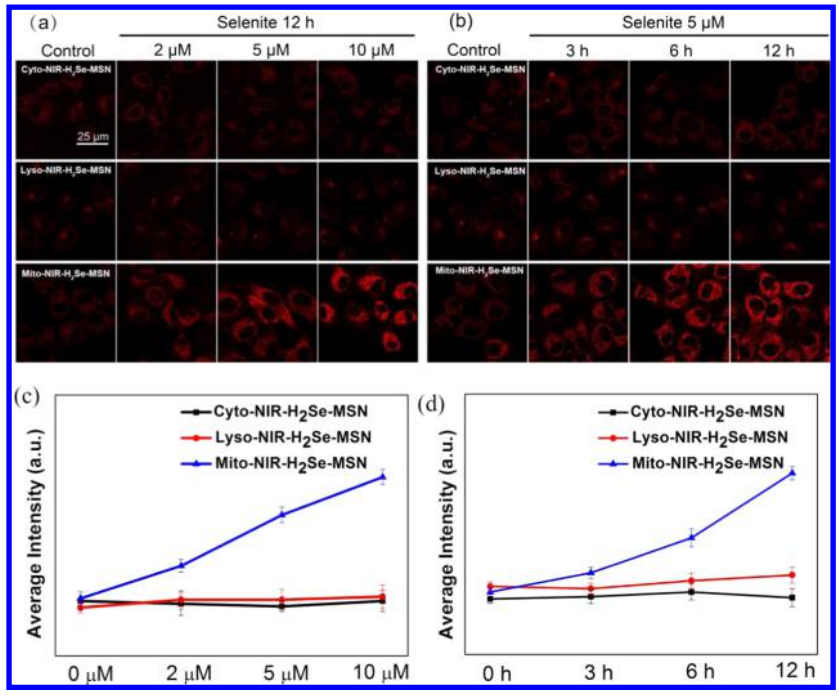


**Figure 5.** CLSM images of endogenous $H_2Se$ in cytoplasm, lysosome, and mitochondria treated with $Na_2SeO_3$ under hypoxic (1% $pO_2$) conditions. (a) The fluorescence changes for HepG2 cells incubated with 0−10 $\mu$M $Na_2SeO_3$ for 12 h and incubated with the three nanoprobes (0.1 mg/mL). (b) The fluorescence changes of HepG2 cells incubated with 5 $\mu$M of $Na_2SeO_3$ for 0−12 h and incubated with the three nanoprobes (0.1 mg/mL). (c, d) The quantitative analyses of the corresponding results.

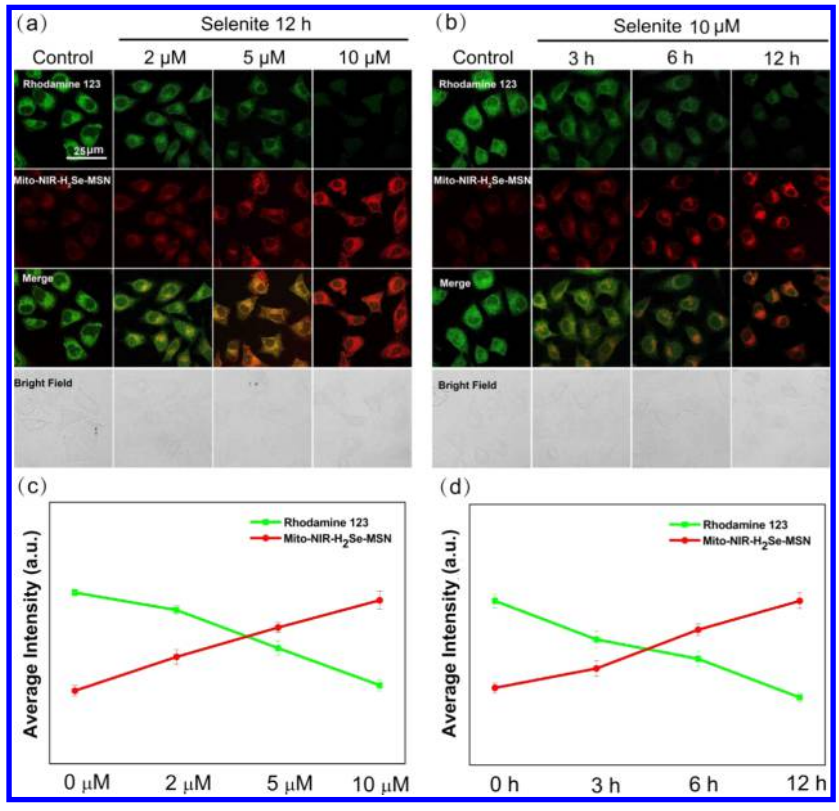


**Figure 6.** (a, b) CLSM images of HepG2 cells incubated with rhodamine 123 and Mito-NIR-$H_2Se$-MSN. (c, d) The quantitative analyses of the corresponding results from (a) and (b).

quite weak. However, in the subcellular targeting moiety-modified nanoplatforms, CF-640, a bright and acid resistance NIR fluorescent dye instead of NIR-$H_2Se$, was loaded to improve the veracity in the colocalization experiments. Calcein (AC), Lyso-Tracker Green (LTG), and Mito-Tracker Green (MTG) are commercially available targeting dyes for cytoplasm, lysosomes, and mitochondria, respectively. The Cyto-CF-640-MSN, Lyso-CF-640-MSN, and Mito-CF-640-


DOI: 10.1021/acsami.8b02206
ACS Appl. Mater. Interfaces 2018, 10, 17345−17351

MSN were coincubated for 6 h with HepG2, HeLa, and MCF-7 cells, respectively, and before CLSM imaging, relevant organelles were labeled with commercially available dyes. In Figure 4, a well-overlapped image was obtained for each nanoprobe and organelle dye in HepG2 cells (Pearson's correlation coefficient, $\rho$, $A = 0.652$, $B = 0.572$, $C = 0.786$). And the similar phenomenon was observed in HeLa and MCF-7 cells (Figures S11 and S12). The organelle localizations of the three nanoprobes in HepG2 cells were also observed by TEM (Figure S13). These results proved that the three nanoprobes are effective tools for targeting organelles.

In our previous work, higher $H_2Se$ content was observed in HepG2 cells when $Na_2SeO_3$ was induced under hypoxic conditions, exhibiting a positive correlation with the cell death level.[9] However, because the distribution of $H_2Se$ in the subcellular organelles is still unclear, it becomes a huge obstacle to fully elucidate the biological functions of $H_2Se$ in $Na_2SeO_3$ anticancer signaling pathways. Therefore, the detection of $H_2Se$ in subcellular organelles was examined in HepG2, Hela, and MCF-7 cells. The $Na_2SeO_3$ was incubated with the cells for different incubation time or concentrations (Figure 5), and followed by coincubation with Cyto-NIR-$H_2Se$-MSN, Lyso-NIR-$H_2Se$-MSN, and Mito-NIR-$H_2Se$-MSN for 6 h. In Figure 5, relatively weak fluorescence intensities were observed in the three groups of the stained HepG2 cells, which have not been treated with $Na_2SeO_3$. Nevertheless, the intracellular fluorescence from Mito-NIR-$H_2Se$-MSN-stained cells performed much stronger intensity when the cells were induced by $Na_2SeO_3$ for a longer time or a higher concentration, demonstrating that higher amount of $H_2Se$ only accumulated in mitochondria, rather than cytoplasm or lysosome. Similarly, with the increasing incubation concentration of $Na_2SeO_3$, the fluorescence was obviously enhanced only in mitochondria. The accumulation of $H_2Se$ in mitochondria was also evaluated in HeLa and MCF-7 cells (Figures S14 and S15).

As mitochondria plays a crucial role in regulating cell death, selenite-induced $H_2Se$ accumulation in mitochondria was investigated to check damaged mitochondria's function. The change of mitochondrial membrane potential (MMP) can be monitored using rhodamine 123 staining, which was an early event in apoptosis process triggered by mitochondria. Figure 6 shows that treatment of HepG2 cells with selenite displayed higher amount of $H_2Se$ accumulation in mitochondria and induced a significant loss of MMP. The same tendency was observed in HeLa and MCF-7 cells (Figures S16 and S17). These suggest that in $Na_2SeO_3$-stimulated cancer cells, selenite-induced $H_2Se$ accumulation triggers functional and structural disruption in mitochondria that leads to cell's apoptosis and death.

## CONCLUSIONS

In summary, three MSN-based nanoprobes were developed for understanding the distribution of subcellular $H_2Se$ among corresponding organelles. These nanoprobes own excellent sensitivity to $H_2Se$ and high selectivity over other interferes. In vitro experiments indicated the nanoprobes' decent biocompatibility and targeting for cytoplasm, lysosomes, and mitochondria in living cells. Furthermore, in $Na_2SeO_3$-stimulated cancer cells, $H_2Se$ only can be detected in mitochondria was verified for the first time. In addition, clear evidence of $H_2Se$ accumulation induced by selenite-triggered functional and structural disruption in mitochondria was obtained, which leads to cell apoptosis. These findings offer novel tools to understand the underlying mechanisms of cell death in cancer cells induced by $Na_2SeO_3$ under hypoxic conditions and offer new perspectives for future clinical cancer therapies.

## ASSOCIATED CONTENT

### Supporting Information

The Supporting Information is available free of charge on the ACS Publications website at DOI: 10.1021/acsami.8b02206.

Characterization of the three nanoprobes, the kinetics study, the selectivity of the three nanoprobes for $H_2Se$, the MTT assay, endocytic inhibition studies, TEM images (PDF)

## AUTHOR INFORMATION


### Corresponding Authors

*E-mail: xukehua@sdnu.edu.cn (K.X.).
*E-mail: tangb@sdnu.edu.cn (B.T.).

### ORCID

Bo Tang: 0000-0002-8712-7025


### Author Contributions

The manuscript was written through contributions of all authors. All authors have given approval to the final version of the manuscript.

### Author Contributions

†B.H. and R.C. contributed equally to this work

### Notes

The authors declare no competing financial interest.

## ACKNOWLEDGMENTS

This work was supported by National Natural Science Foundation of China (21535004, 91753111, 21390411, 21775091, 21575081, 21507075, and 21705098).

## REFERENCES


(1) Letavayová, L.; Vlčková, V.; Brozmanová, J. Selenium: From Cancer Prevention to DNA Damage. *Toxicology* **2006**, *227*, 1−14.

(2) Weekley, C. M.; Harris, H. H. Which Form is That? The Importance of Selenium Speciation and Metabolism in the Prevention and Treatment of Disease. *Chem. Soc. Rev.* **2013**, *42*, 8870−8894.

(3) Tarze, A.; Dauplais, M.; Grigoras, I.; Lazard, M.; Ha-Duong, N. T.; Barbier, F.; Blanquet, S.; Plateau, P. Extracellular Production of Hydrogen Selenide Accounts for Thiol-assisted Toxicity of Selenite Against Saccharomyces Cerevisiae. *J. Biol. Chem.* **2007**, *282*, 8759−8767.

(4) Roman, M.; Jitaru, P.; Barbante, C. Selenium Biochemistry and Its Role for Human Health. *Metallomics* **2014**, *6*, 25−54.

(5) Ip, C.; Hayes, C.; Budnick, R. M.; Ganther, H. E. Chemical Form of Selenium, Critical Metabolites, and Cancer Prevention. *Cancer Res.* **1991**, *51*, 595−600.

(6) Liu, Y.; Meng, F.; He, L.; Liu, K.; Lin, W. A Dual-Site Two-Photon Fluorescent Probe for Visualizing Lysosomes and Tracking Lysosomal Hydrogen Sulfide with Two Different Sets of Fluorescence Signals in the Living Cells and Mouse Liver Tissues. *Chem. Commun.* **2016**, *52*, 7016−7019.

(7) Yuan, L.; Wang, L.; Agrawalla, B. K.; Park, S.; Zhu, H.; Sivaraman, B.; Peng, J.; Xu, Q.; Chang, Y. Development of Targetable Two-Photon Fluorescent Probes to Image Hypochlorous Acid in Mitochondria and Lysosome in Live Cell and Inflamed Mouse Model. *J. Am. Chem. Soc.* **2015**, *137*, 5930−5938.

(8) Wu, C.-L.; Zhao, Y. CdS Quantum Dots as Fluorescence Probes for the Sensitive and Selective Detection of Highly Reactive $HSe^-$ Ions in Aqueous Solution. *Anal. Bioanal. Chem.* **2007**, *388*, 717−722.




DOI: 10.1021/acsami.8b02206
ACS Appl. Mater. Interfaces 2018, 10, 17345−17351

(9) Kong, F.; Ge, L.; Pan, X.; Xu, K.; Liu, X.; Tang, B. A Highly Selective Near-Infrared Fluorescent Probe for Imaging $H_2Se$ in Living Cells and in Vivo. *Chem. Sci.* **2016**, *7*, 1051−1056.
(10) Li, Y.; Li, N.; Pan, W.; Yu, Z.; Yang, L.; Tang, B. Hollow Mesoporous Silica Nanoparticles with Tunable Structures for Controlled Drug Delivery. *ACS Appl. Mater. Interfaces* **2017**, *9*, 2123−2129.
(11) Wu, S.; Hung, Y.; Mou, C. Compartmentalized Hollow Silica Nanospheres Templated from Nanoemulsions. *Chem. Mater.* **2013**, *25*, 352−364.
(12) Li, Y.; Chen, Y.; Pan, W.; Yu, Z.; Yang, L.; Wang, H.; Li, N.; Tang, B. Nanocarriers with Multi-Locked DNA Valves Targeting Intracellular Tumor-Related mRNAs for Controlled Drug Release. *Nanoscale* **2017**, *9*, 17318−17324.
(13) An, J.; Yang, X.; Cheng, K.; Song, X.; Zhang, L.; Li, C.; Zhang, X.; Xuan, Y.; Song, Y.; Fang, B.; Hou, X.; Zhao, Y.; Liu, B. In Vivo Computed Tomography/Photoacoustic Imaging and NIR-Triggered Chemo−Photothermal Combined Therapy Based on a Gold Nanostar-, Mesoporous Silica-, and Thermosensitive Liposome-Composited Nanoprobe. *ACS Appl. Mater. Interfaces* **2017**, *9*, 41748−41759.
(14) Li, Z.; Barnes, J. C.; Bosoy, A.; Stoddart, J. F.; Zink, J. I. Mesoporous Silica Nanoparticles in Biomedical Applications. *Chem. Soc. Rev.* **2012**, *41*, 2590−2605.
(15) Wang, X.-H.; Peng, H. S.; Yang, L.; You, F. T.; Teng, F.; Hou, L. L.; Wolfbeis, O. S. Targetable Phosphorescent Oxygen Nanosensors for the Assessment of Tumor Mitochondrial Dysfunction By Monitoring the Respiratory Activity. *Angew. Chem., Int. Ed.* **2014**, *53*, 12471−12475.
(16) Zhang, K.; Xu, L. L.; Jiang, J. G.; Calin, N.; Lam, K. F.; Zhang, S. J.; Wu, H. H.; Wu, G. D.; Albela, B.; Bonneviot, L.; Wu, P. Facile Large-Scale Synthesis of Monodisperse Mesoporous Silica Nanospheres with Tunable Pore Structure. *J. Am. Chem. Soc.* **2013**, *135*, 2427−2430.
(17) Kojima, H.; Nakatsubo, N.; Kikuchi, K.; Kawahara, S.; Kirino, Y.; Nagoshi, H.; Hirata, Y.; Nagano, T. Detection and Imaging of Nitric Oxide with Novel Fluorescent Indicators: Diaminofluoresceins. *Anal. Chem.* **1998**, *70*, 2446−2453.
(18) Gilleron, J.; Querbes, W.; Zeigerer, A.; Borodovsky, A.; Marsico, G.; Schubert, U.; Manygoats, K.; Seifert, S.; Andree, C.; Stoter, M.; Epstein-Barash, H.; Zhang, L.; Koteliansky, V.; Fitzgerald, K.; Fava, E.; Bickle, M.; Kalaidzidis, Y.; Akinc, A.; Maier, M.; Zerial, M. Image-based Analysis of Lipid Nanoparticle−Mediated siRNA Delivery, Intracellular Trafficking and Endosomal Escape. *Nat. Biotechnol.* **2013**, *31*, 638−646.
(19) Chen, H.; Xiao, L.; Anraku, Y.; Mi, P.; Liu, X.; Cabral, H.; Inoue, A.; Nomoto, T.; Kishimura, A.; Nishiyama, N.; Kataoka, K. Polyion Complex Vesicles for Photoinduced Intracellular Delivery of Amphiphilic Photosensitizer. *J. Am. Chem. Soc.* **2014**, *136*, 157−163.
(20) Yu, Z.; Sun, Q.; Pan, W.; Li, N.; Tang, B. A Near-Infrared Triggered Nanophotosensitizer Inducing Domino Effect on Mitochondrial Reactive Oxygen Species Burst for Cancer Therapy. *ACS Nano* **2015**, *9*, 11064−11074.
(21) Huth, U. S.; Schubert, R.; Peschka-Suss, R. Investigating the Uptake and Intracellular Fate of pH-Sensitive Liposomes by Flow Cytometry and Spectral Bio-imaging. *J. Controlled Release* **2006**, *110*, 490−504.
(22) Lai, S. K.; Hida, K.; Man, S. T.; Chen, C.; Machamer, C.; Schroer, T. A.; Hanes, J. Privileged Delivery of Polymer Nanoparticles to the Perinuclear Region of Live Cells via a non-Clathrin, non-Degradative Pathway. *Biomaterials* **2007**, *28*, 2876−2884.
(23) Raghu, H.; Sharma-Walia, N.; Veettil, M. V.; Sadagopan, S.; Chandran, B. Kaposi's Sarcoma-Associated Herpesvirus Utilizes an Actin Polymerization-Dependent Macropinocytic Pathway To Enter Human Dermal Microvascular Endothelial and Human Umbilical Vein Endothelial Cells. *J. Virol.* **2009**, *83*, 4895−4911.
(24) Ganther, H. E. Reduction of the Selenotrisulfide Derivative of Glutathione to a Persulfide Analog by Glutathione Reductase. *Biochemistry* **1971**, *10*, 4089−4098.
(25) Fairweather-Tait, S. J.; Bao, Y.; Broadley, M. R.; Collings, R.; Ford, D.; Hesketh, J. E.; Hurst, R. Selenium in Human Health and Disease. *Antioxid. Redox Signaling* **2011**, *14*, 1337−1383.
(26) Wallenberg, M.; Olm, E.; Hebert, C.; Bjornstedt, M.; Fernandes, A. P. Selenium Compounds are Substrates for Glutaredoxins: a Novel Pathway for Selenium Metabolism and a Potential Mechanism for Selenium-Mediated Cytotoxicity. *Biochem. J.* **2010**, *429*, 85−93.
(27) Kong, F.; Hu, B.; Gao, Y.; Xu, K.; Pan, X.; Huang, F.; Zheng, Q.; Chen, H.; Tang, B. Fluorescence Imaging of Selenol in HepG2 Cell Apoptosis Induced by $Na_2SeO_3$. *Chem. Commun.* **2015**, *51*, 3102−3105.
(28) Ly, J. D.; Grubb, D. R.; Lawen, A. The Mitochondrial Membrane Potential ($\Delta\psi$m) in Apoptosis; an Update. *Apoptosis* **2003**, *8*, 115−128.
(29) Bao, Y.; De Keersmaecker, H.; Corneillie, S.; Yu, F.; Mizuno, H.; Zhang, G.; Hofkens, J.; Mendrek, B.; Kowalczuk, A.; Smet, M. Tunable Ratiometric Fluorescence Sensing of Intracellular pH by Aggregation-Induced Emission-Active Hyperbranched Polymer Nanoparticles. *Chem. Mater.* **2015**, *27*, 3450−3455.
(30) Li, Y.; Wang, Y.; Yang, S.; Zhao, Y.; Yuan, L.; Zheng, J.; Yang, R. Hemicyanine-based High Resolution Ratiometric near-Infrared Fluorescent Probe for Monitoring pH Changes in Vivo. *Anal. Chem.* **2015**, *87*, 2495−2503.
(31) Marín, M. J.; Galindo, F.; Thomas, P.; Russell, D. A. Localized Intracellular pH Measurement Using a Ratiometric Photoinduced Electron-Transfer-Based Nanosensor. *Angew. Chem., Int. Ed.* **2012**, *51*, 9657−9661.
(32) Stinchcombe, J.; Bossi, G.; Griffiths, G. M. Linking Albinism and Immunity: The Secrets of Secretory Lysosomes. *Science* **2004**, *305*, 55−59.
(33) Chen, Y.; Zhu, C.; Cen, J.; Bai, Y.; He, W.; Guo, Z. Ratiometric Detection of pH Fluctuation in Mitochondria with a New Fluorescein/Cyanine Hybrid Sensor. *Chem. Sci.* **2015**, *6*, 3187−3194.
(34) Turk, B.; Turk, V. Lysosomes as "Suicide Bags" in Cell Death: Myth or Reality? *J. Biol. Chem.* **2009**, *284*, 21783−21787.
(35) Cao, L.; Zhao, Z.; Zhang, T.; Guo, X.; Wang, S.; Li, S.; Li, Y.; Yang, G. In Vivo Observation of the pH Alternation in Mitochondria for Various External Stimuli. *Chem. Commun.* **2015**, *51*, 17324−17327.
(36) Wu, M. Y.; Li, K.; Liu, Y. H.; Yu, K. K.; Xie, Y. M.; Zhou, X. D.; Yu, X. Q. Mitochondria-Targeted Ratiometric Fluorescent Probe for Real Time Monitoring of pH in Living Cells. *Biomaterials* **2015**, *53*, 669−678.
(37) Llopis, J.; McCaffery, J. M.; Miyawaki, A.; Farquhar, M. G.; Tsien, R. Y. Measurement of Cytosolic, Mitochondrial, and Golgi pH in Single Living Cells with Green Fluorescent Proteins. *Proc. Natl. Acad. Sci. U.S.A.* **1998**, *95*, 6803−6808.


DOI: 10.1021/acsami.8b02206
*ACS Appl. Mater. Interfaces* 2018, 10, 17345−17351